Contract No:

This document was prepared in conjunction with work accomplished under Contract No. DE-AC09-08SR22470 with the U.S. Department of Energy (DOE) Office of Environmental Management (EM).

Disclaimer:

August 26th 2015 SRNL-STI-2015-00437

Subject: SRNL CRP Progress Report

From: J. W. Amoroso
J. C. Marra

Melt Processed Crystalline Ceramic Waste Forms for Advanced Nuclear Fuel Cycles

CRP T21027 1813: Processing technologies for high level waste, formulation of matrices and characterization of waste forms, Task 17208: Final Report

1.0 Abstract

A multi-phase ceramic waste form is being developed at the Savannah River National Laboratory (SRNL) for treatment of secondary waste streams generated by reprocessing commercial spent nuclear. The envisioned waste stream contains a mixture of transition, alkali, alkaline earth, and lanthanide metals. Ceramic waste forms are tailored (engineered) to incorporate waste components as part of their crystal structure based on knowledge from naturally found minerals containing radioactive and non-radioactive species similar to the radionuclides of concern in wastes from fuel reprocessing. The ability to tailor ceramics to mimic naturally occurring crystals substantiates the long term stability of such crystals (ceramics) over geologic timescales of interest for nuclear waste immobilization [1]. A durable multi-phase ceramic waste form tailored to incorporate all the waste components has the potential to broaden the available disposal options and thus minimize the storage and disposal costs associated with aqueous reprocessing. This report summarizes results from three years of work on the IAEA Coordinated Research Project on "Processing technologies for high level waste, formulation of matrices and characterization of waste forms" (T21027), and specific task "Melt Processed Crystalline Ceramic Waste Forms for Advanced Nuclear Fuel Cycles" (17208).

2.0 Introduction

Savannah River National Laboratory (SRNL) is developing melt-processed reference ceramic waste forms for treatment of waste streams generated by reprocessing commercial spent nuclear fuel. The waste form is designed to crystallize upon cooling from a melt (melt-processing) into a multiphase ceramic. Melt processing of waste forms is considered advantageous over the conventional solid-state synthesis methods given that melters are currently in use for HLW vitrification in several countries, greatly facilitating the technology readiness of ceramic waste forms, and melter technology can reduce the potential for airborne contamination during pretreatment as compared to processes involving extensive powder handling operations.

Ceramic waste forms are tailored (engineered) to incorporate waste components as part of their crystal structure based on knowledge from naturally found minerals containing radioactive and non-radioactive species similar to the radionuclides of concern in wastes from fuel reprocessing. The ability to tailor ceramics to mimic naturally occurring crystals substantiates the long term stability of such crystals (ceramics) over geologic timescales of interest for nuclear waste immobilization [1]. A durable multi-phase ceramic waste form tailored to incorporate all the waste components has the potential to broaden the available disposal options and thus minimize the storage and disposal costs associated with aqueous reprocessing. Compositions are designed based on combinations of the waste and additives to target desired hollandite, perovskite, and pyrochlore phases. Elements with a +3 or +2 valance form perovskite ($(A^{+2})TiO_3$) and pyrochlore ($(A^{+3})_2Ti_2O_7$) type phases.[1,2] Zirconium (+4 valence) partitions to a zirconolite ($CaZrTi_2O_7$) phase.[3] Cs and Rb elements partition to a hollandite structure based on the general formula $Ba_xCs_yM_zTi^{+4}_{8-z}O_{16}$ where z = 2x+y for trivalent cations and z = x+y/2 for divalent cations for charge compensation.[4-6]

There have been several comparative studies of crystalline ceramic waste forms produced by hot pressing and inductive melting [7,8]. These prior studies have indicated that the specimens fabricated by melting and solid state sintering exhibited similar mineral compositions. Under oxidizing processing conditions, attempts to make single phase hollandite (the host phase for Cs) ceramics are difficult and secondary metastable Cs containing phases are formed [4]. In particular, water-soluble cesium molybdate phases observed in melt processing Mo containing waste in air are undesirable. It has been demonstrated that these secondary phases can be suppressed by controlling the starting composition and the Ti^{3+}/Ti^{4+} during processing. Metal powder (Ti) additions to the batch material or hot pressing in graphite have been shown to be effective methods for controlling the redox conditions during sintering [9,10].

Idaho National Laboratory (INL) recently (October 2014) conducted a cold crucible induction melter (CCIM) test with a ceramic waste form (non-radioactive) developed at SRNL to demonstrate proof of principle for processing multi-phase crystalline waste forms from a melt. Prior to the CCIM testing, property data (e.g., high temperature viscosity and electrical conductivity) was collected for two potential test compositions. One, designated 'Fe-MP' was designed towards optimized processing and the other, designated 'CAF 5%TM MP' was designed towards optimized phase formation. The Fe-MP composition is an early developed composition that suffers from improper phase assemblage, but melts a relativey low composition and was expected to be adequate for processing in the CCIM as currently configured at INL. The CAF-5%TM-MP composition was formulated based on a baseline Cr/Al/Fe-based hollandite composition but with 5% addition of transition metal (TM) elements in an effort to enhance melt-ability for processing in the CCIM. The CAF-5%TM-MP composition forms more-desirable phases upon cooling but melts at temperatures that would test the limits of INL's CCIM as configured at the time.[9]

It was recommended, and ultimately decided to perform initial CCIM testing using the Fe-MP composition with the intention to gather information regarding the performance of the melter, particularly with regard to processing a ceramic material (which had not yet been performed with INL's CCIM) to be used to support subsequent CCIM testing with more ideal feed compositions. During this initial test, the drain operation could not be completed and instead of casting the ceramic into a mold, the melt was allowed to cool to room temperature in the melter. Subsequently, core samples were taken of the material remaining in the CCIM after cooling and characterized.

The information presented in this report summarizes results and outcomes from this project over the last three years aimed at

- developing a reference crystalline ceramic composition and melt process for HLW waste streams of interest to U.S. DOE-NE for potential commercial fuel recycling (Year 1),
- understanding the impact of compositional changes to the reference composition in terms of process parameters and product properties (Year 2), and
- pilot scale melter testing and analysis of crystalline ceramic waste forms processed using
- CCIM technology.

3.0 Composition Development

3.1 Projected Waste Composition

The waste composition that formed the basis for the development and testing is given in Table 1. Noble metals, minor actinides and Tc were removed for cost and handling reasons. The MoO_3 targeted in this work was based on one possible reprocessing flowsheet, but other variants exist and more will be developed based in part on waste form studies such as this. Because this work incorporated varying redox conditions and previous results indicated large concentrations of MoO_3 inhibited desired phase formation under oxidizing conditions, the MoO_3 concentration was targeted at 3 wt. % to simplify comparison among samples.

Table 1. Projected and re-normalized waste composition targeted in this study

Group	Fuel[a]	SRNL[b]	Fuel[c]
Alkali	7.6	13.4	9.6
Alkaline Earth	8.3	12.9	10.6
Lanthanides	33.1	51.8	42.0
Actinides	4.0	-	-
Noble Metals	14.6	-	-
MoO_3	13.7	3.4	17.4
ZrO_2	13.7	12.1	17.4
TcO_2	2.7	-	-
Others	2.4	6.3	3.0
Total	100	100	100

[a]Projection

[b]Does not include corrosion and process products

[c]Renormalized to exclude corrosion and process products

3.2 Hollandite Phase Development

Cs is one of the more problematic fission product radionuclides to immobilize due to its high volatility, ability to form water soluble compounds, and its mobility in many host materials. There are natural analogues of hollandite including ankagite, found in dolomitic marble in the Apuan Alps in Tuscany, Italy which demonstrate the long term stability of these crystal structures over geologic timescales [11]. The hollandite group of minerals has the formula $A_xB_yC_{8-y}O_{16}$ where the B and C cations are surrounded by octahedral configuration of oxygen [12]. In the hollandite structure, columns of four pairs of edge sharing octahedra connected to each other on the corners form tunnels running parallel to the short crystal axis. The tunnel cross-section is generally square, but will distort as a rhombus depending on the particular Hollandite symmetry which can be either monoclinic (rhombus) or tetragonal (square) depending on the radius ratio of the A to B site cations. Figure 1 depicts a two-dimensional schematic of the tetragonal hollandite structure. In hollandite structures used for nuclear waste incorporation, the A site is occupied by Cs/Rb and Ba, the B site by Al^{3+} and Ti^{+3}, and the C site by Ti^{+4} resulting in the general formula of $(Ba_xCs_y)(Ti,Al)^{+3}_{2x+y}(Ti^{+4}_{8-2x-y})O_{16}$ [13].

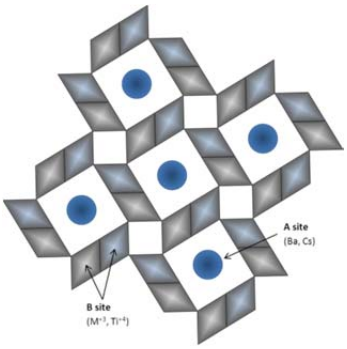

Figure 1. Idealized two-dimensional [001] projection of the tetragonal hollandite structure showing octahedra pairs lining the tunnels and A site cation positions.

3.3 Calculation of Multi Phase Waste Form Compositions

Single phase hollandite compositions based on Cr and Cr/Al/Fe additions were incorporated into multiphase ceramics targeting hollandite, perovskite/pyrochlore and zirconolite phase assemblages. The phase assemblages were designed based on combinations of the waste and additives (the primary additive being TiO_2) to target the desired phases (i.e. hollandite, perovskite/pyrochlore and zirconolite) upon melting and subsequent cooling.

Table 2 summarizes two multiphase compositions (based on Cr and Cr/Al/Fe single phase hollandite studies) that were prepared, each with ~25 weight % waste loading and varying additive concentrations. Cr-MP denotes a multiphase assemblage targeting the Cr-hollandite analog and CAF-MP denotes a multiphase assemblage targeting the Cr/Al/Fe-hollandite analog.

Table 2. Additive and waste concentrations (wt. %) of multiphase melt samples.

	Target wt. %		Target Phase
	CAF-MP	Cr-MP	
Waste	***24.66***	***24.58***	
BaO	2.20	2.20	**Cs-Hollandite** $(Ba_xCs_y)(Ti,Al)^{+3}_{2x+y}(Ti^{+4}_{8-2x-y})O_{16}$
CdO	0.11	0.11	-
Ce_2O_3	3.10	3.09	**(2+/3+) Titanate (i.e. Perovskite / Pyrochlore)** $(A^{2+})TiO_3$; $(A^{3+})_2Ti_2O_7$
Cs_2O	2.88	2.87	**(2+/3+) Titanate (i.e. Perovskite / Pyrochlore)** $(A^{2+})TiO_3$; $(A^{3+})_2Ti_2O_7$
Eu_2O_3	0.17	0.17	**(2+/3+) Titanate (i.e. Perovskite / Pyrochlore)** $(A^{2+})TiO_3$; $(A^{3+})_2Ti_2O_7$
Gd_2O_3	0.16	0.16	**(2+/3+) Titanate (i.e. Perovskite / Pyrochlore)** $(A^{2+})TiO_3$; $(A^{3+})_2Ti_2O_7$
La_2O_3	1.58	1.58	**(2+/3+) Titanate (i.e. Perovskite / Pyrochlore)** $(A^{2+})TiO_3$; $(A^{3+})_2Ti_2O_7$
MoO_3	0.85	0.84	-
Nd_2O_3	5.23	5.22	**(2+/3+) Titanate (i.e. Perovskite / Pyrochlore)** $(A^{2+})TiO_3$; $(A^{3+})_2Ti_2O_7$
Pr_2O_3	1.45	1.44	**(2+/3+) Titanate (i.e. Perovskite / Pyrochlore)** $(A^{2+})TiO_3$; $(A^{3+})_2Ti_2O_7$
Rb_2O	0.42	0.42	**Cs-Hollandite** $(Ba_xCs_y)(Ti,Al)^{+3}_{2x+y}(Ti^{+4}_{8-2x-y})O_{16}$
SeO_2	0.08	0.08	-
Sm_2O_3	1.08	1.07	**(2+/3+) Titanate (i.e. Perovskite / Pyrochlore)** $(A^{2+})TiO_3$; $(A^{3+})_2Ti_2O_7$
SnO_2	0.07	0.07	**(4+) Zirconolite** $CaZrTi_2O_7$
SrO	0.98	0.98	**(2+/3+) Titanate (i.e. Perovskite / Pyrochlore)** $(A^{2+})TiO_3$; $(A^{3+})_2Ti_2O_7$
TeO_2	0.66	0.65	-
Y_2O_3	0.63	0.63	**(2+/3+) Titanate (i.e. Perovskite / Pyrochlore)** $(A^{2+})TiO_3$; $(A^{3+})_2Ti_2O_7$
ZrO_2	2.99	2.98	**(4+) Zirconolite** $CaZrTi_2O_7$
Additive	***75.34***	***75.42***	
Al_2O_3	1.27	0.00	**Cs-Hollandite** $(Ba_xCs_y)(Ti,Al)^{+3}_{2x+y}(Ti^{+4}_{8-2x-y})O_{16}$
CaO	1.39	1.38	**(4+) Zirconolite** $CaZrTi_2O_7$
Cr_2O_3	6.33	14.50	**Cs-Hollandite** $(Ba_xCs_y)(Ti,Al)^{+3}_{2x+y}(Ti^{+4}_{8-2x-y})O_{16}$
BaO	10.56	10.52	**Cs-Hollandite** $(Ba_xCs_y)(Ti,Al)^{+3}_{2x+y}(Ti^{+4}_{8-2x-y})O_{16}$
Fe_2O_3	6.65	0.00	**Cs-Hollandite** $(Ba_xCs_y)(Ti,Al)^{+3}_{2x+y}(Ti^{+4}_{8-2x-y})O_{16}$
TiO_2	49.16	49.01	**Various**

4.0 Single Phase Hollandite Crucible Studies

Cs-containing hollandite ceramics with Cr additions of the form $Ba_{1.0}Cs_{0.3}A_{2.3}Ti_{5.7}O_{16}$ (A = Cr, Fe, Al) were developed precursory to multiphase work. Cr-containing hollandite was developed to exploit the relative thermodynamic stability of Cr oxides and the Cr ionic radius that is less than Fe^{3+} but greater than Al^{3+}. Three nominal hollandite compositions, $Ba_{1.0}Cs_{0.3}Cr_{2.3}Ti_{5.7}O_{16}$ – referred to as Cr-Hol, $Ba_{1.0}Cs_{0.3}Cr_{1.0}Al_{0.3}Fe_{1.0}Ti_{5.7}O_{16}$ – referred to as CAF-Hol, and $Ba_{1.0}Cs_{0.3}Fe_{2.3}Ti_{5.7}O_{16}$ – referred to as Fe-Hol were prepared and characterized. In addition, the waste stream is anticipated to contain MoO_3 which is known to preferentially react with Cs_2O and it is recognized that reducing atmospheres are a proven method to suppress Cs-Mo secondary phase formation. Based on that expectation, a variety of reducing conditions were evaluated including the use of solid state reducing agents (Ti/TiO_2) and reducing gas environments ($1\%H_2/Ar$). The approach in this precursory work was to study an additive (Cr) that promoted single phase hollandite formation and Cs incorporation across a wide range of redox conditions thus resulting in a flexible Cs immobilization host material that could be incorporated into a multiphase ceramic.

4.1 Preparation and Processing

For each composition, stoichiometric amounts of reagent-grade oxide and carbonate powders (99.5 % purity) to make 100 g of hollandite material were combined in a 500 ml plastic bottle with zirconia milling media, filled 2/3 full with deionized water, and agitated in a tumbler mixer for 1 hour. Subsequently, each slurry was poured into a separate pan along with additional rinse water used to collect any batch material remaining on the milling media and bottles. Each pan was transferred to an oven where the slurry was dried for several days at 90°C. The dried material was bagged and used as feed stock for synthesis experiments.

Approximately 20 g samples feed stock was placed loosely into a covered alumina crucible. The samples were heated in air and in 1% H_2 (99% Ar) reducing atmosphere. Ti metal and TiO_2 additions were made to some batches prior to synthesis. For those samples, prepared mixtures of 2.0 wt. % Ti metal and 7.0 wt. % TiO_2 were manually mixed into each batch. Samples were heated at approximately 15 K/min, held at 1500 °C for 20 minutes, and furnace cooled (powered off furnace). Table 3 summarizes the experimental matrix including TiO_2 additions and processing conditions.

Table 3. Composition, Additive, and Processing Atmosphere Experimental Matrix

Target Hollandite Composition	Additive	Atmosphere	Short Identifier
$Ba_{1.0}Cs_{0.3}Fe_{2.3}Ti_{5.7}O_{16}$	Ti-TiO_2	Air	Fe-SPH-Ti
		Reduced (1%H_2)	Fe-SPHR-Ti
	n/a	Air	Fe-SPH
		Reduced (1%H_2)	Fe-SPHR
$Ba_{1.0}Cs_{0.3}Cr_{2.3}Ti_{5.7}O_{16}$	Ti-TiO_2	Air	Cr-SPH-Ti
		Reduced (1%H_2)	Cr-SPHR-Ti
	n/a	Air	Cr-SPH
		Reduced (1%H_2)	Cr-SPHR
$Ba_{1.0}Cs_{0.3}Cr_{1.0}Al_{0.3}Fe_{1.0}Ti_{5.7}O_{16}$	Ti-TiO_2	Air	CAF-SPH-Ti
		Reduced (1%H_2)	CAF-SPHR-Ti
	n/a	Air	CAF-SPH
		Reduced (1%H_2)	CAF-SPHR

4.2 Results

4.2.1 X-ray diffraction

The phases identified by XRD are summarized and presented in
Table 4. All Cr-Hol samples were single phase except the sample heated in air to which Ti/TiO_2 was added, which contained excess rutile (TiO_2). This was not unexpected, as excess TiO_2 was intentionally added and similar results have been reported by other groups. All CAF-Hol samples exhibited a major hollandite phase, but also contained minor titanate phases. In contrast, the Fe-Hol samples, although exhibiting a major hollandite phase, also contained several parasitic phases including titanatates and aluminates. The majority of the detected parasitic phases would be expected to be durable. However, one phase, $CsAlTiO_4$ was also detected and is known to adversely affect Cs retention when subjected to a durability test.

Table 4. Summary of Crystalline phases determined from X-ray Diffraction XRD measurements and Energy Dispersive X-ray Spectroscopy EDAX elemental analysis

Short ID	Major Phase[1]	Minor Phase(s)[2]	Processing Conditions
Fe-SPH	Hollandite	$Fe_2Ti_3O_9$; $CsTiAlO_4$	Air
Fe-SPH-Ti	Hollandite	$Fe_3Ti_3O_{10}$; $CsTiAlO_4$	Air w/Ti-TiO_2
Fe-SPHR	Hollandite	$BaFe_{12}O_{19}$; $CsTiAlO_4$; $FeAl_2O_4$	1% H_2
Fe-SPHR-Ti	Hollandite	Al_2O_3; $FeAl_2O_4$	1% H_2 w/Ti-TiO_2
Cr-SPH	Hollandite		Air
Cr-SPH-Ti	Hollandite	TiO_2	Air w/Ti-TiO_2
Cr-SPHR	Hollandite		1% H_2
Cr-SPHR-Ti	Hollandite		1% H_2 w/Ti-TiO_2
CAF-SPH	Hollandite		Air
CAF-SPH-Ti	Hollandite	TiO_2	Air w/Ti-TiO_2
CAF-SPHR	Hollandite	Fe_2TiO_4; $BaFe_{12}O_{19}$; $CsTiAlO_4$	1% H_2
CAF-SPHR-Ti	Hollandite	Fe_2TiO_4	1% H_2 w/Ti-TiO_2

[1] Many hollandite phases exist in the literature. In general, the following PDF files were used to identify the hollandite phases: Fe: 00-051-1900; Cr: 00-039-0352, CAF: 01-076-3178.

[2] The following PDF files were used to identify the minor phases: TiO_2: 00-021-1276; $BaFe_{12}O_{19}$: 00-039-1433; Fe_2TiO_4: 00-034-0177; $FeAl_2O_4$: 01-086-2320; $CsTiAlO_4$: 04-009-3837 $Fe_3Ti_3O_{10}$: 00-047-0421; $Fe_2Ti_3O_9$: 00-0407-1777; Al_2O_3: 00-005-0712

4.2.2 Electron microscopy

Microstructures of the single phase hollandite compositions are shown in Figure 2. Overall, the observed microstructures confirm the XRD results indicating that the Cr-hol samples were single hollandite phase, the CAF-Hol samples exhibited a major hollandite phase accompanied by minor phases, and the Fe-hol samples were multiphase. Semi-quantitative EDS confirmed the composition of many of the various phases. CAF-Hol samples were characterized further with high resolution transmission electron microscopy (HRTEM) and SEM. Figure 3, which shows the HRTEM results for the CAF-Hol sample heated in air, indicated the hollandite phase was highly crystalline and contained all the expected elements including Cs. The selected area diffraction (SAD) pattern shown in the inset was indexed to a tetragonal hollandite phase. Elemental maps of the Al, Cs, Fe, and Cr concentrations of Cr/Al/Fe-hol samples heated in 1%H_2 *with and without* Ti/TiO_2 are presented in Figure 4. The Cr-rich phase was identified as the primary hollandite phase. Fe partitioned mainly to a reduced titanate phase in both samples, but was also distributed along hollandite grain boundaries in the sample processed *without* Ti/TiO_2 additions. The Cs was associated with the Al in the CAF-Hol sample heated in 1%H_2 *without* Ti-TiO_2 and is the characteristic bright phase in SEM identified as $CsAlTiO_4$. In contrast, the Cs appeared more distributed in the CAF-Hol sample heated under the same atmosphere, but *with* Ti/TiO_2 additions.

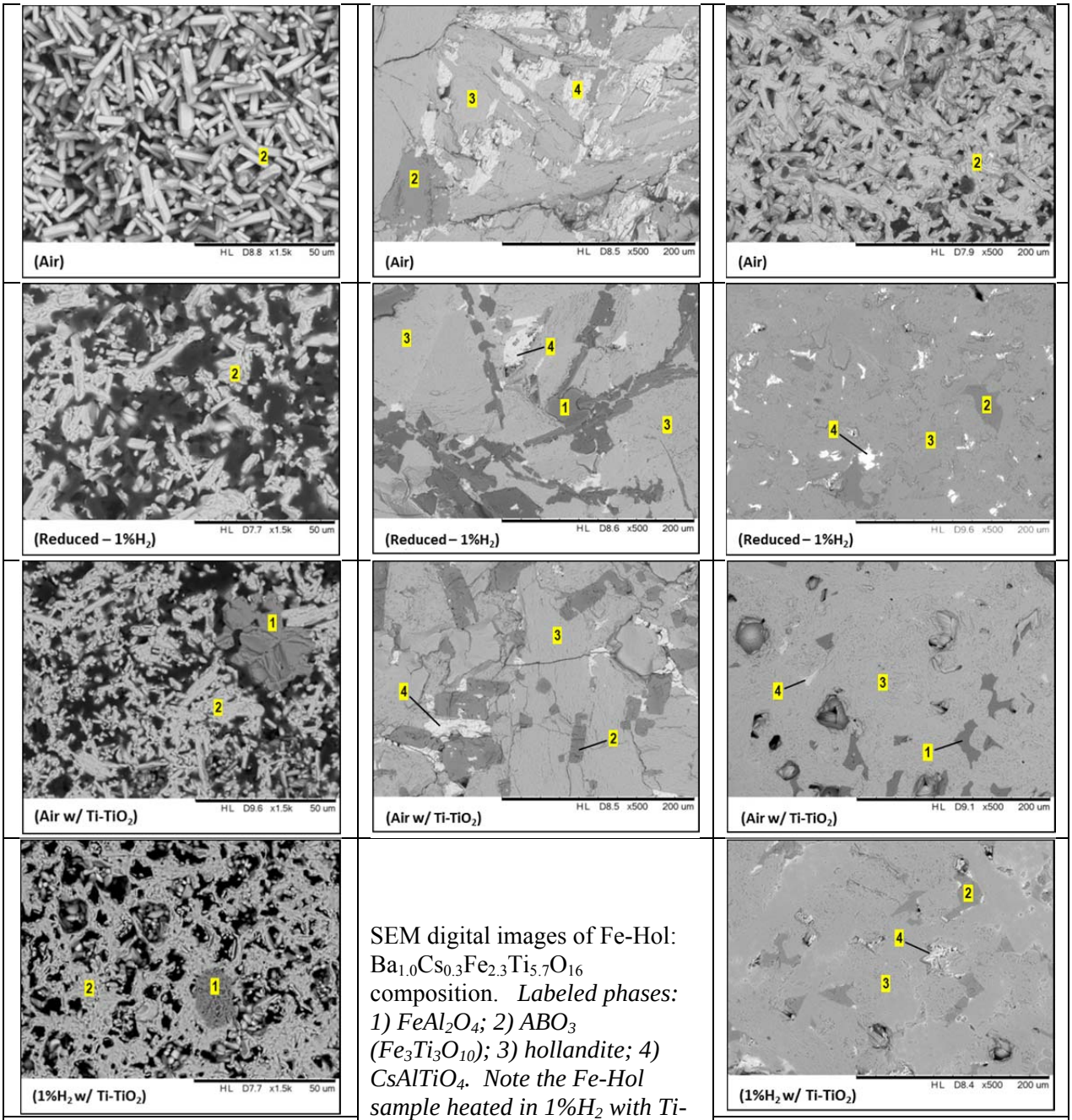

SEM digital images of Cr-Hol: $Ba_{1.0}Cs_{0.3}Cr_{2.3}Ti_{5.7}O_{16}$ composition. *Labeled phases: 1) rutile; 2) hollandite.*

SEM digital images of Fe-Hol: $Ba_{1.0}Cs_{0.3}Fe_{2.3}Ti_{5.7}O_{16}$ composition. *Labeled phases: 1) $FeAl_2O_4$; 2) ABO_3 ($Fe_3Ti_3O_{10}$); 3) hollandite; 4) $CsAlTiO_4$. Note the Fe-Hol sample heated in 1%H_2 with Ti-TiO_2 was unrecoverable from the furnace*

SEM digital images of CAF-Hol: $Ba_{1.0}Cs_{0.3}Cr_{1.0}Al_{0.3}Fe_{1.0}Ti_{5.7}O_{16}$ composition. *Labeled phases: 1) rutile; 2) Fe_2TiO_4; 3) hollandite; 4) $CsAlTiO_4$.*

Figure 2. SEM back scattered detector (BSD) digital images of single phase hollandite samples.

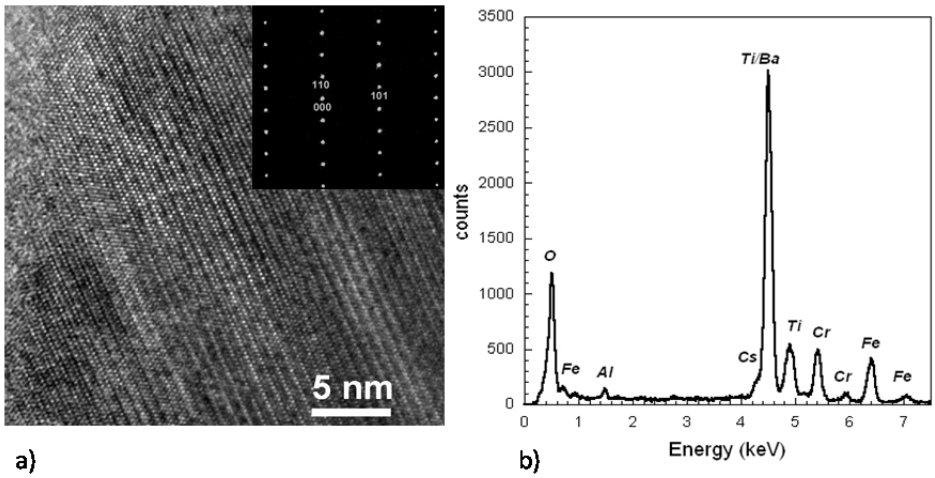

Figure 3. HRTEM image of CAF-SPH melted in Air without Ti/TiO_2 (inset SAD indexed to a tetragonal crystal structure) and b) chemical composition.

Details of elemental analysis is described elsewhere[14] but, in summary, data form single phase experiments indicates that Cr preferentially enters the hollandite phase (even in the presence of competing phases). Due to its refractory nature, Cr does not form compounds readily with Cs and Cr^{3+} is not easily susceptible to reduction. Cr_2O_3 appears to stabilize the hollandite phase which in turn should promote Cs incorporation. This is visually observed in the SEM images by comparing the relative area of bright phase ($CsAlTiO_4$) across all samples and within each composition group.

4.2.3 Durability Measurements

A standardized durability measurement has yet to be developed for multiphase ceramic waste forms. Leaching tests were performed to assess the comparative Cs retention between the three hollandite compositions synthesized under various processing conditions. The leaching test was intended to provide a qualitative measure of the Cs incorporation into the various hollandite compositions based on the assumption that parasitic Cs-rich phases control the initial Cs loss in leach tests. The measured Cs release was normalized to the measured surface area (0.1 – 0.4 m^2/g) for each sample. The Cs release across the samples for a given processing route was then normalized to one. The normalized Cs release summarized in Figure 4, indicated that the Fe-Hol sample exhibited the least Cs retention whereas the Cr-Hol sample exhibited the greatest Cs retention. The addition of Ti/TiO_2 appeared to increase the Cs retention in the Cr and CAF samples (to clarify, the increase was measured for the same processing atmosphere, not across air and 1%H_2). The Cs retention was greater in samples not heated under reducing conditions. This result can be understood considering the characterization results, which indicated reducing environments favor secondary phase formation that compete for Cs retention with the hollandite.

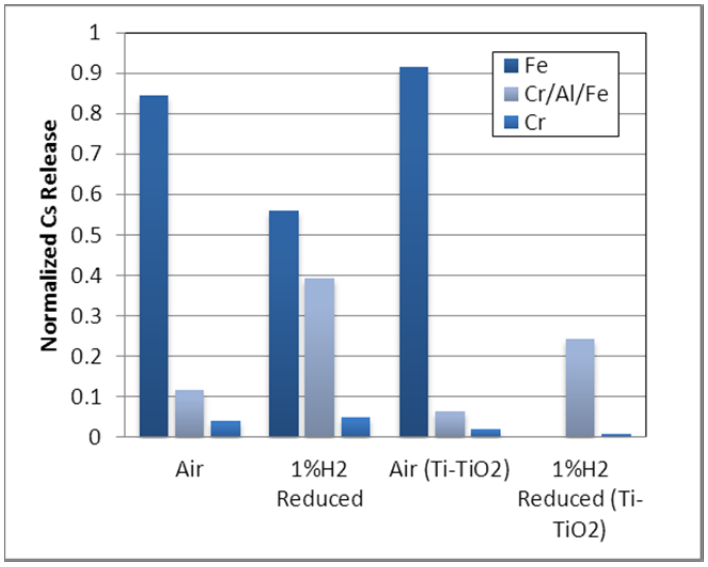

Figure 4. Normalized Cs release for Fe-Hol: $Ba_{1.0}Cs_{0.3}Fe_{2.3}Ti_{5.7}O_{16}$ (Fe), CAF-Hol: $Ba_{1.0}Cs_{0.3}Cr_{1.0}Al_{0.3}Fe_{1.0}Ti_{5.7}O_{16}$ (CAF), and, Cr-Hol: $Ba_{1.0}Cs_{0.3}Cr_{2.3}Ti_{5.7}O_{16}$ (Cr).

5.0 Multiphase Ceramic Crucible Studies

Multiphase ceramics were tested based on single phase hollandite results. Two nominal hollandite compositions, $Ba_{1.0}Cs_{0.3}Cr_{2.3}Ti_{5.7}O_{16}$ – referred to as *Cr-Hol* and $Ba_{1.0}Cs_{0.3}Cr_{1.0}Al_{0.3}Fe_{1.0}Ti_{5.7}O_{16}$ – referred to as *CAF-Hol*, and $Ba_{1.0}Cs_{0.3}Fe_{2.3}Ti_{5.7}O_{16}$ were incorporated into multiphase compositions and are designated *Cr-MP* and CAF-MP, respectively.

5.1 Preparation and Processing

For each batch, stoiciometric amounts of reagent-grade oxide and carbonate powders (99.5 % purity to make 100 g of final material were combined in a 500 ml plastic bottle with zirconia milling media, filled 2/3 full with deionized water, and agitated in a tumbler mixer for 1 hour. Subsequently, the slurry was poured into a pan along with additional rinse water used to collect any batch material remaining on the milling media and bottles. The pan was transferred to an oven where the slurry was dried for several days at 90°C. The dried material was bagged and used as feed stock for synthesis experiments.

Approximately 20 g samples feed stock was placed loosely into a covered alumina crucible. Samples were heated at approximately 15 K/min, held at 1500°C for 20 minutes, and furnace cooled (powered off furnace). Estimated cooling rates were initially 60 K/min but had reduced to 15 K/min by approximately 1200°C. The samples were heated in air and in 1% H_2 ¬(99% Ar) reducing atmosphere. Ti metal and TiO_2 additions were made to some batches prior to synthesis. For those samples, mixtures of 2.0 wt. % Ti metal and 7.0 wt. % TiO_2 were weighed in an inert glove box and manually mixed into each batch prior to melting summarizes the experimental matrix including TiO_2 additions and processing conditions.

Table 5. Multiphse experimental matrix and processing conditions.

Composition ID[a]	TiO_2 Buffer	Atmosphere	Sample-ID
Cr-MP	No	Air	Cr-MP
		1% H_2	Cr-MP-R
	Yes	Air	Cr-MP-Ti
		1% H_2	Cr-MP-R-Ti
CAF-MP	No	Air	CAF-MP
		1% H_2	CAF-MP-R
	Yes	Air	CAF-MP-Ti
		1% H_2	CAF-MP-R-Ti

[a] "Cr-…" targeted $Ba_{1.0}Cs_{0.3}\mathbf{Cr}_{2.3}Ti_{5.7}O_{16}$ Hollandite;
"CAF-…" targeted $Ba_{1.0}Cs_{0.3}\mathbf{Cr}_{1.0}\mathbf{Al}_{0.3}\mathbf{Fe}_{1.0}Ti_{5.7}O_{16}$ Hollandite.

5.2 Results

5.2.1 X-ray Diffraction

The names perovskite and pyrochlore used in this context describe the more general $ATiO_3$ and $A_2B_2O_6/A_2B_2O_7$ (where A and B are rare-earth and transition metal cations) type compounds, respectively. The structures of those compounds are highly substitutional, can accommodate multiple cation species on lattice sites, and depend on the cation species and concentration in the compound. All of these factors add complexity to the XRD pattern, and indeed many possible 2+/3+ titanate (pyrochlore/perovskite) phases could be identified in the XRD patterns. For the purposes of this work, XRD was used only as a gross assessment of the phases. Detailed structure refinements are needed to fully assess the waste-form which, are outside the scope of this work, but will be pursued in subsequent research.

XRD confirmed that the samples were, in general, multiphase assemblages of the target phases. Table 6 summarizes phases identified in the XRD patterns after melt processing. The XRD results indicate that reducing conditions significantly affect the resulting phase assemblages during melt processing. It is known that titanium oxygen equilibrium reactions impact the hollandite stoichiometry in sintered SYNROC materials [10]. In this work, adjustments to the Ti^{3+}/Ti^{4+} ratio made by adding Ti metal to control the hollandite stoichiometry resulted in greater Cs retention as expected. Fe_2O_3 is also relatively easily reduced and impacted phase assemblage during melt processing. Under reducing conditions Fe species reacted with the crucible and other primary phase constituents as evidenced by the resulting amount of excess Al and parasitic Fe-containing phases.

Noticeable differences in phase assemblage were measured between samples processed in air to those processed in 1% H_2. A $Sr_3Mo_2O_7$ (pdf 00-052-1252) double layered perovskite phase was noted as a possible phase in Cr samples produced in 1% H_2 suggesting that Mo may enter a perovkite phase under reducing conditions, which would support previous evidence that reducing conditions suppress Cs-Mo containing phases. Mo containing perovskites are known to exist and recent research on the irradiation of the $Sr_2Fe_{1.5}Mo_{0.5}O_{6-\delta}$ perovskite compound indicated that Mo containing perovskites could be potential waste form materials [15]. This suggests that processing in 1% H_2 suppresses Cs-Mo containing phases and promotes Mo partitioning to a durable phase. The appearance of Ba-Al-O compounds under air environments indicates that at least a portion of the Ba reacts with Al_2O_3. However, the presence of

excess Al_2O_3 (assumed from reaction with the crucible) would suggest that its reaction with Ba was limited, perhaps due to the high temperature stability of the Cr hollandite phase.

Table 6. Phases Identified in Multiphase Ceramics after Processing.

Short Identifier	Phases				Processing Conditions
	Cs-Hollandite	(4+) Zirconolite	(2+/3+) Titanate	Other	
Cr-MPB1A	X	X	X	$Ba_7Al_2O_{10}$ Al_2O_3 TiO_2	Air
Cr-MPB1A-Ti	X	X	X	$Ba_7Al_2O_{10}$ Al_2O_3 TiO_2	Air w/Ti-TiO_2
Cr-MPB1R	X	X	X	$Sr_3Mo_2O_7$	1% H_2
Cr-MPB1R-Ti	X	X	X	$Sr_3Mo_2O_7$ TiO_2	1% H_2 w/Ti-TiO_2
CAF-MPB1A	X	X	X	$Ba_7Al_2O_{10}$	Air
CAF-MPB1A-Ti	X	X	X	$Ba_7Al_2O_{10}$ Al_2O_3 TiO_2	Air w/Ti-TiO_2
CAF-MPB1R	X	X	X	$BaFe_{12}O_{19}$ Unidentified	1% H_2
CAF-MPB1R-Ti	X	X	X	$Ba_7Al_2O_{10}$ $BaFe_{12}O_{19}$ FeO Unidentified	1% H_2 w/Ti-TiO_2

5.2.2 Electron Microscopy

Representative back scattered electron (BSE) SEM images of each sample after melt processing are presented in Figure 5. Similar phases were identified in all samples. The most abundant mid tone gray corresponds to hollandite phase and the lighter tone gray phase that is also relatively abundant corresponds to pyrochlore and perovskite phases. The darker phases correspond to pores and other minor phases including TiO_2 and Al_2O_3. More specific phases are identified and labeled in Figure 6 for the samples processed in 1% H_2 with Ti-TiO_2 additions. The microstructures presented in Figure 6 are higher magnification images representative of the melt processing process. Overall, the observed microstructures confirm the XRD results as evidenced by characteristic contrast in the images taken using the BSD mode and semi-quantitative EDS. Excess Al_2O_3 and TiO_2 were also identified in the Cr/Al/Fe and Cr samples respectively, in agreement with the XRD results and processing conditions. The morphology between the Cr and Cr/Al/Fe samples was also different. The Cr samples exhibited relatively small but dispersed phases whereas the Cr/Al/Fe samples exhibited larger but less dispersed phases in agreement with the processing observations and the high refractory nature of the Cr sample.

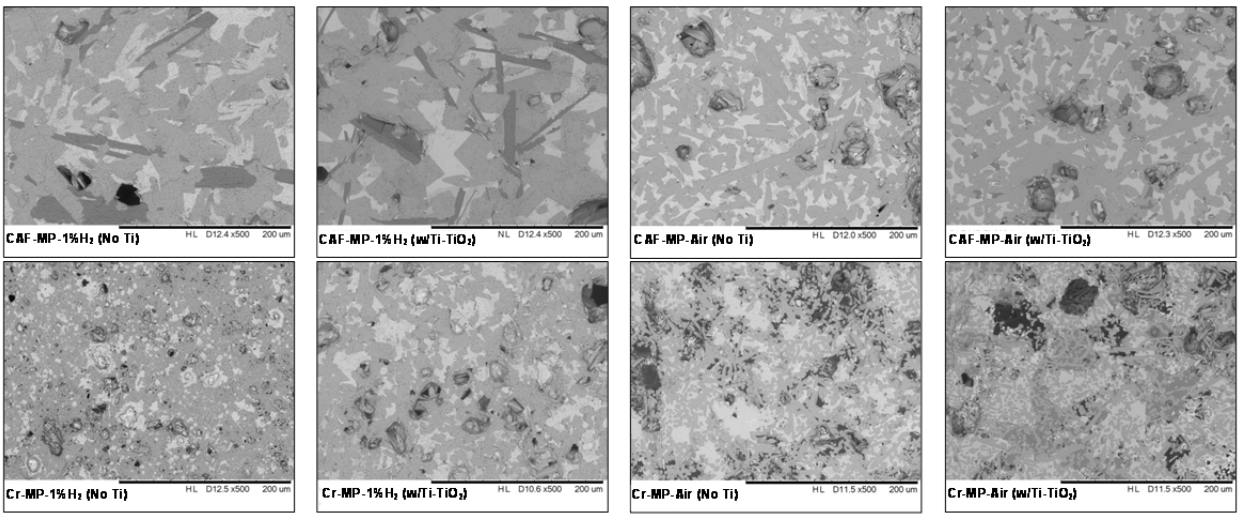

Figure 5. Digital SEM images of melt processed multi-phase ceramics.

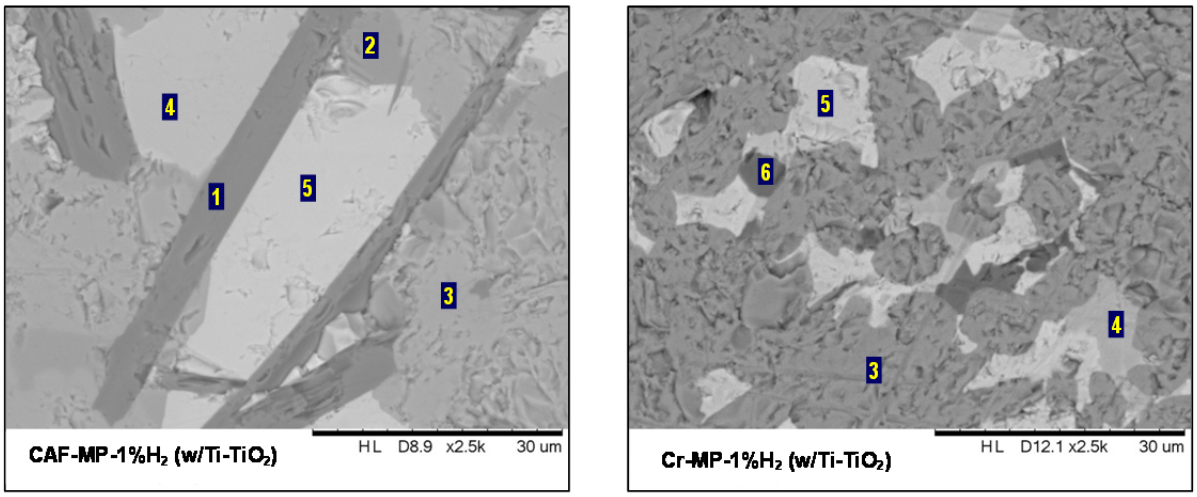

Figure 6. SEM back scattered detector (BSD) digital images taken of each composition processed in 1%H_2 with Ti–TiO_2. Labeled phases: (1) Al_2O_3; (2) FeO (possible); (3) hollandite, (4) Zirconolite, 5) Perovskite/Pyrochlore $(A^{+3}_xB^{+2}_{1-x})TiO_3$, and 6) rutile.

The Cr/Al/Fe samples processed with Ti-TiO_2 were further examined using STEM-EDS to identify minor phases not observed in XRD or SEM and to probe elemental partitioning within the various phases. Figure 7 shows select elemental maps taken for the Cr/Al/Fe samples processed 1% H_2 with Ti-TiO_2 additions. Distinct phases are evident in the EDS maps and some elements appeared to partition more so than others. Cr is primarily associated with the hollandite phase, as would be expected from previous work and XRD results that indicated the high stability of the Cr-hollandite analog [14]. Zr appeared to be associated with Ca and Nd. Ca likely is associated with a zirconolite phase and a $(A^{3+})_{0.4}Ca_{0.4}TiO_3$ perovskite, both of which were identified in the XRD patterns. Nd may also be associated with $Nd_2Zr_2O_7$ phase, a pyrochlore similar to $Y_2Ti_2O_7$ identified in the XRD patterns. Evidence of a $Nd_2Zr_2O_7$ phase

indicates that Zr – rare-earth pyrochlore is viable host for those waste elements without the needed Ca additions to form zirconolite.

Fe appeared to be concentrated at the hollandite grain boundaries (compare Cr and Fe maps) in the Cr/Al/Fe sample processed in 1% H_2 supporting the XRD data and in agreement with previous single-phase hollandite results [14]. Fe, thought to be one of the more reactive and mobile species in the composition, was generally confined to the hollandite phase (compare Cr and Fe maps) in the sample but exhibited noticeable concentration gradients. Mo and Cs appeared to be distributed throughout with no visually obvious Cs-Mo. (Typically, Cs_2MoO_4 would appear much brighter and with a different color (additive)) This indicates that reducing atmosphere is effective in reducing (if not eliminating) Cs-Mo containing phases.

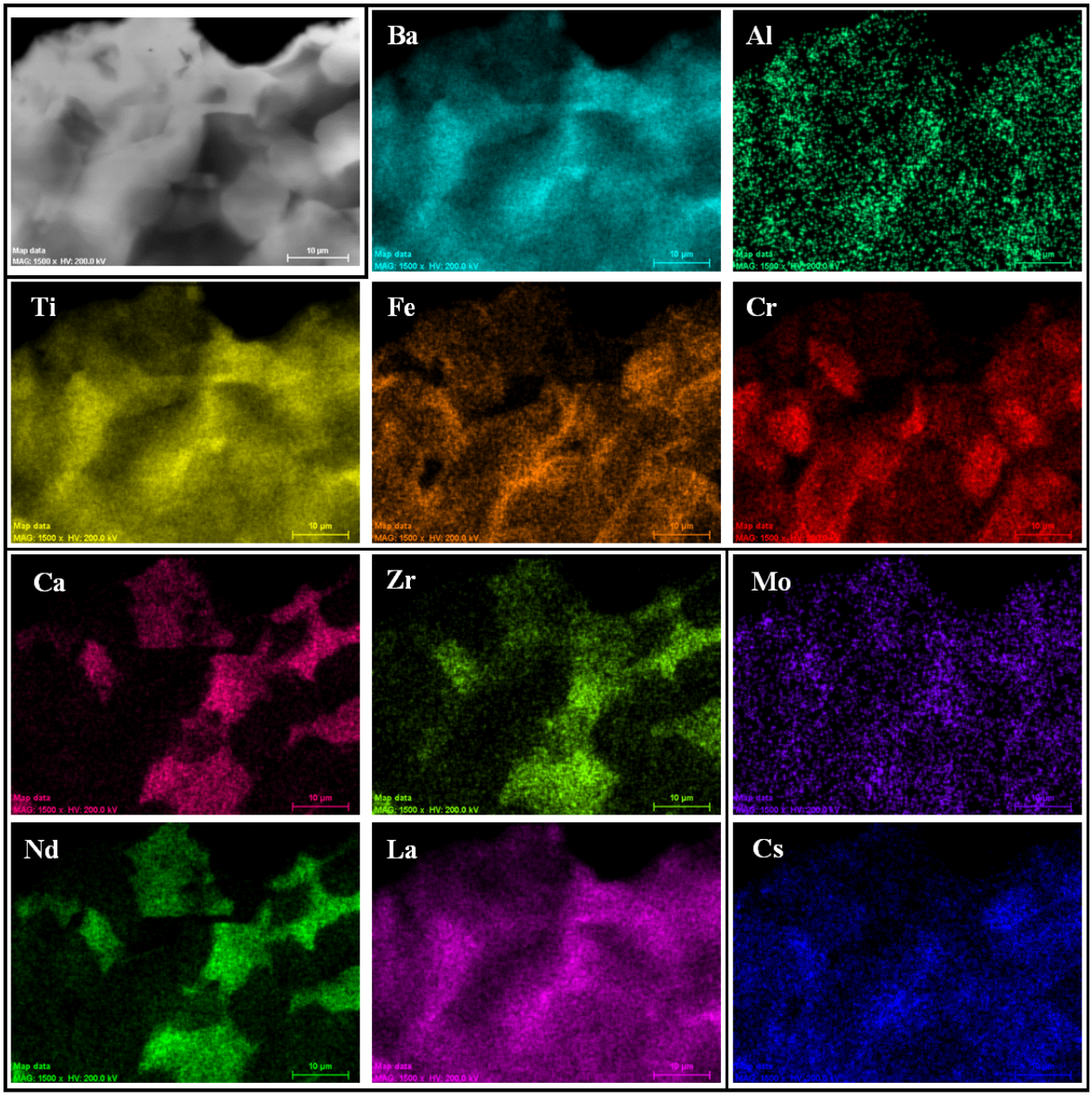

Figure 7. STEM-EDS elemental mapping measurements of Cr/Al/Fe multi-phase composition processed in 1% H_2 with Ti-TiO_2. (All maps are scaled identically: refer to contrast image for scale bar (10μm))

6.0 Pilot Scale CCIM Demonstration

6.1 CCIM Test Summary[a]

INL personnel melted and attempted to pour a ceramic waste form composition using the CCIM. The feed material for the CCIM was supplied by Mo-Sci Corporation (Rolla, MO) as a dry stoichiometric mixture of oxide and carbonate reagents totaling ~30 kg. SRNL performed chemical analysis to confirm the feed material composition prior to use. The targeted and measured elemental and feed chemical concentrations are listed in Table 7. In general, the prepared feed measured composition was within typical analytical uncertainty of the target composition.

Table 7. Target and Measured Elemental Concentrations (wt. %) in CCIM Feed Material.

	Target	Measured
Ba	10.69	10.25
Ca	0.93	0.91
Cd	0.09	0.04
Ce	2.48	2.43
Cs	2.54	2.19
Eu	0.14	0.17
Fe	10.00	9.76
Gd	0.13	0.13
La	1.26	1.17
Mo	0.53	0.37
Nd	4.19	3.74
Pr	1.16	1.18
Rb	0.36	n.m.
Se	0.05	<0.10
Sm	0.87	0.90
Sn	0.05	0.09
Sr	0.78	1.01
Te	0.49	0.55
Ti	27.55	27.15
Y	0.46	0.44
Zr	2.07	1.98
Sum[b]	66.8	64.5

Batch Chemical	Target	Calculated
$BaCO_3$	15.36	14.72
$CaCO_3$	2.31	2.28
CdO	0.10	0.05
CeO_2	3.05	2.98
Cs_2CO_3	3.11	2.69
Eu_2O_3	0.16	0.19
Fe_2O_3	14.29	13.95
Gd_2O_3	0.15	0.15
La_2O_3	1.48	1.37
MoO_3	0.79	0.57
Nd_2O_3	4.89	4.37
Pr_6O_{11}	1.40	1.43
Rb_2CO_3	0.49	n.m.
SeO_2	0.08	<0.14
Sm_2O_3	1.01	1.04
SnO_2	0.07	0.11
$SrCO_3$	1.31	1.70
TeO_2	0.61	0.69
TiO_2	45.96	45.31
Y_2O_3	0.59	0.56
ZrO_2	2.79	2.68
Total	100.0	96.8

A Ti initiator ring and approximately 13.5 kg of feed material was packed into the CCIM. This initial charge was approximately 6 inches tall used for primary ignition of the melt. A full melt was achieved in approximately 3 hours at which point additional feed was added at 5.5 kg/hr. The CCIM's RF generator

[a] The experimental parameters and operating conditions during the CCIM test are presented in greater detail elsewhere. (See V. C. Maio, "Production of a Low Temperature SYNROC All Ceramic Surrogate High Level Waste Form in INL's Cold Crucible Induction Melter Pilot –Validation of Test Completion," *U.S. Department of Energy Report INL/MIS-14-34012 (FCRD-SWF-2015-00256),* Idaho National Laboratory, Idaho Falls, ID (2014).)

[b] Measured and calculated values do not include Rb contribution.

was operating at its maximum design power (60 kW) level to maintain the melt and after approximately 40 minutes and 3 kgs[c] of added feed an attempt was made to drain the melter. Nitrogen cooling to the drain assembly was terminated and the drain tube heater was turned on. The heater burnt out in less than five minutes of being turned on. In an attempt to utilize as much latent heat as possible, cooling water to the drain system was decreased, but the system was unable to sustain the lower cooling rate and a leak in the cooling system (presumably from boiling water) triggered the automatic shutdown of the RF generator and termination of the test.

Additional cooling was supplied to the crucible stays in an attempt to increase the temperature gradient across the crucible during cooling so that samples could be subsequently taken having undergone different cooling rates. The estimated cooling time for the center of the melt was approximately 4 hours, or ~ averaged 6 K/min. Obviously, the outer material cooled faster and the water cooled crucible walls could have realistically generated cooling rates in the 100's K/min range. Seven core samples were taken from the solidified melter material and characterized. Characterization results and pertinent experimental procedures are presented subsequently.

6.2 Experimental

6.2.1 Core Sample Preparation

Seven 1-inch diameter core drilled samples were taken from the solidified material in the CCIM. The locations and depth dimensions for the core samples from the melter material are shown in Figure 8 and Table 8. Morphology differences along the vertical axes of the core samples were visually evident in the as-received core samples. In general, three morphologies were evident in each sample; dense, columnar, and porous. These regions were designated Zone 1, Zone 2, and Zone 3, respectively. As many of the cores cracked during drilling, the cores were appropriately reassembled (temporarily held together with super glue) prior to characterization in order to link subsequent results to different areas within each core. Digital images representative of the as-received and cross-sectioned core samples are shown in Figure 9 and Figure 10, respectively.

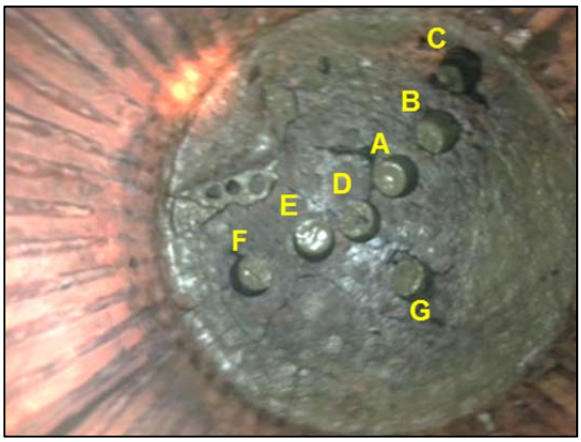

Figure 8. Digital image of solidified material in melter showing core sample locations.

Table 8. Core sample dimensions.

Core	Core Depth (inch)
A	1 3/8
B	1 1/2
C	1 11/16
D	1 3/8
E	2
F	1 5/8
G	1 1/4

[c] Although the feed rate was continuous, the feeder was only run intermittently.

Figure 9. Core sample F as-received after re-assembly.

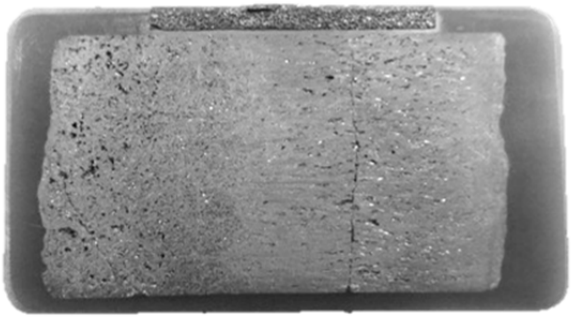

Figure 10. Core sample F cross-section mounted in epoxy.

6.3 Results and Discussion

6.3.1 Chemical Composition

Samples were selectively chosen for chemical analysis and grouped according to visual morphology. Figure 11 is images of a representative core (sample F) in which dense, columnar, and porous morphologies are evident along the length of the core. In general, it was straight-forward to identify and section samples that were either dense or columnar in appearance. Such samples were labeled *Zone 1* and *Zone 2* respectively. It was more difficult to accurately identify porous sections due to a less definitive transition from the columnar morphology to the porous morphology. Therefore, samples that could be identified as porous were sampled and labeled as *Zone 3*. A fourth set of samples consisting of Zone 2 and Zone 3 material where a definitive distinction was difficult to identify were measured and labeled *Zone 5*. One additional sample was measured that was not sectioned prior to analysis, representing the bulk material. In total, 29 samples taken from 4 different cores and from various (~7) bulk regions in the melted CCIM material were analyzed.

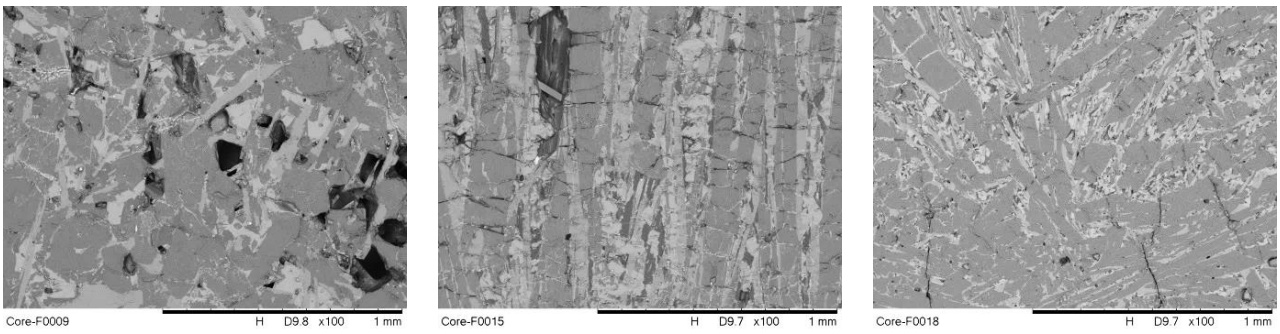

Porous (Zone 3) Columnar (Zone 2) Dense (Zone 1)

Figure 11. SEM phase contrast images that reveal morphology differences along the length of the core sample.

Table 9 lists the measured elemental concentrations in the bulk CCIM material as represented by the sample that was not analyzed by zone. In general, the results indicate that the CCIM material composition was comparable to the target composition excepting Al, Cs, Mo, and Te. Although no Al was added to the CCIM feed material, these materials are known to readily react with available Al_2O_3. It is suspected that much of the Al from the crucible used to hold the initiator ring in place[d] reacted during the CCIM processing and additional Al may also have been introduced from refractory used in the CCIM. Cs is a highly volatile species and previous experiments have generally shown that about 50% of the Cs is lost during heating. However, in this CCIM test, it appears that less Cs was lost, about 32%.[e] Substantial amounts (>70%) of Mo and Te were unaccounted for in the measured analysis.[f] Whereas Cs is known to volatilize, Mo and Te are not known to volatilize at such rates that would explain the results. Ultimately, the fate of the Mo and Te are unknown.

Table 9. Measured elemental concentrations (wt. %) in the bulk CCIM sample that was not analyzed by zone.

Element	Target	Measured
Al	0.00	2.21
Ba	10.69	10.54
Ca	0.93	0.93
Cd	0.09	<0.10
Ce	2.48	2.47
Cs	2.54	1.73
Eu	0.14	0.12
Fe	10.00	9.88
Gd	0.13	0.12
La	1.26	1.22
Mo	0.53	0.15
Nd	4.19	4.02
Pr	1.16	1.21
Rb	0.36	n.m.
Se	0.05	<0.10
Zr	2.07	1.97
Sm	0.87	0.85
Sn	0.05	n.m.
Sr	0.78	0.99
Te	0.49	0.13
Ti	27.55	30.13
Y	0.46	0.40

Chemical composition was also measured as a function of Zone and radial location. Figure 12 shows the measured elemental concentration means for each Zone with corresponding standard error bars. In

[d] Refer to reference in footnote a for a discussion of the initiator ring setup.
[e] Table 1 indicates the feed material could have been deficient in Cs and Mo by as much as ~15% and ~30%, respectively. Therefore, the Cs (and Mo) retention would be greater than if calculated from Table 3.

general, chemical composition did not appear to depend on the zone from which the material came, indicating that the CCIM material was relatively homogeneous. However, the data shown in Figure 12 do appear to indicate greater variation in the means of the measured values for Al[g] and the lanthanide series elements. Analysis of variance (ANOVA) was used to test for statistically significant differences in the data between zones. The results of the ANOVA indicated statistically significant differences (at the 5% significance level) for Ce, La, Nd, Pr, Sr, and Te. Specifically, the means for Ce, La, and Pr were not statistically significant between zones 1, 2, and 5, or between zones 3 and 5 (i.e. Zone 5 is common). Similarly, the means for Nd and Sr were not statistically significant between zones 1, 2, and 5 or between zones 2, 3, and 5 (i.e. zone 2 and 5 are common). The means for Te were not statistically significant between zones 1, 3, and 5 and there was no common connection to zone 2.

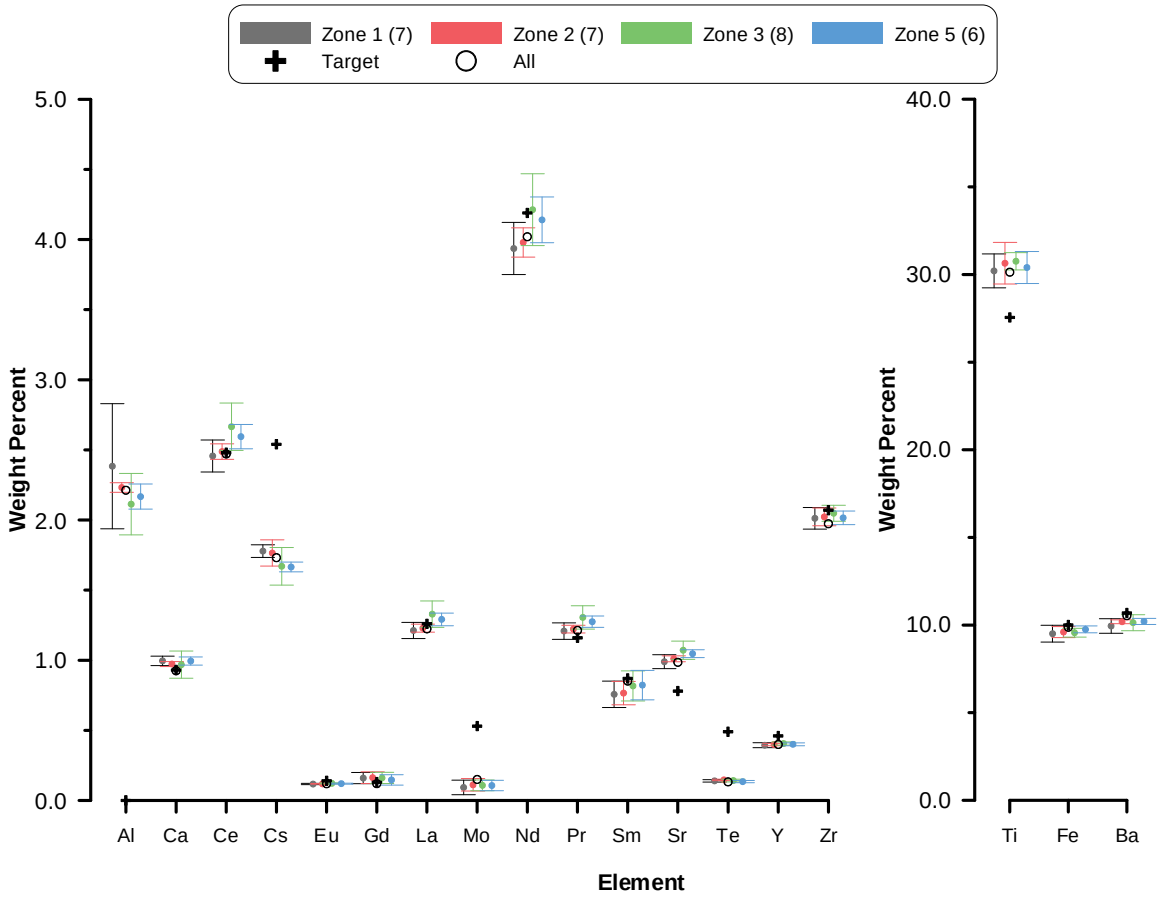

Figure 12. Plot of mean elemental concentrations and corresponding standard deviation from samples grouped according to morphology (Zone) type.

In practical terms, the ANOVA results, the subjectivity involved with differentiating distinct boundaries between zones (morphology transitions, in particular between zone 3 and 2, hence the use of zone 5), and

[g] The variance in the Al concentration is unknown.. However, closed-end Al_2O_3 cylinders were used to support a Ti initiator ring during processing that were observed to significantly react with the feed material as evidenced by one of the supports having been found to be significantly dissolved compared to its initial dimensions.. It is possible that some samples were taken nearer those Al_2O_3 supports than other samples and thus would have relatively increased Al concentration.

microscopy results indicate most lanthanide series elements are likely distributed less uniformly than other elements. Nevertheless, the magnitude of those differences remains small; the elemental variances shown in Figure 12 are typically less than 0.5 wt. %.

Figure 13 shows the same composition data as that shown in Figure 12 except the data is grouped according to core sample, or radial position from the center of the melter. In general, smaller standard errors (relative to the Zone analysis) were observed across cores excepting core F, which exhibited the greatest variation. The variation in Core F measurements is attributed to Zone 3 measurements in which many of the lanthanide series elements were the greatest of all the samples in the study.[h] This result further supports the previous conclusion that lanthanide series elements were distributed less homogeneously than other elements, particularly in the porous regions of the CCIM ceramic material. Given that Core F was also located near the edge of the crucible, it is possible that cooling differences or interactions with the cold wall of the melter may influence elemental partitioning. Overall, the chemical composition measurements were remarkably consistent. The data confirms that the CCIM mixes the melt very well and demonstrates the melt was homogenous both radially and vertically.

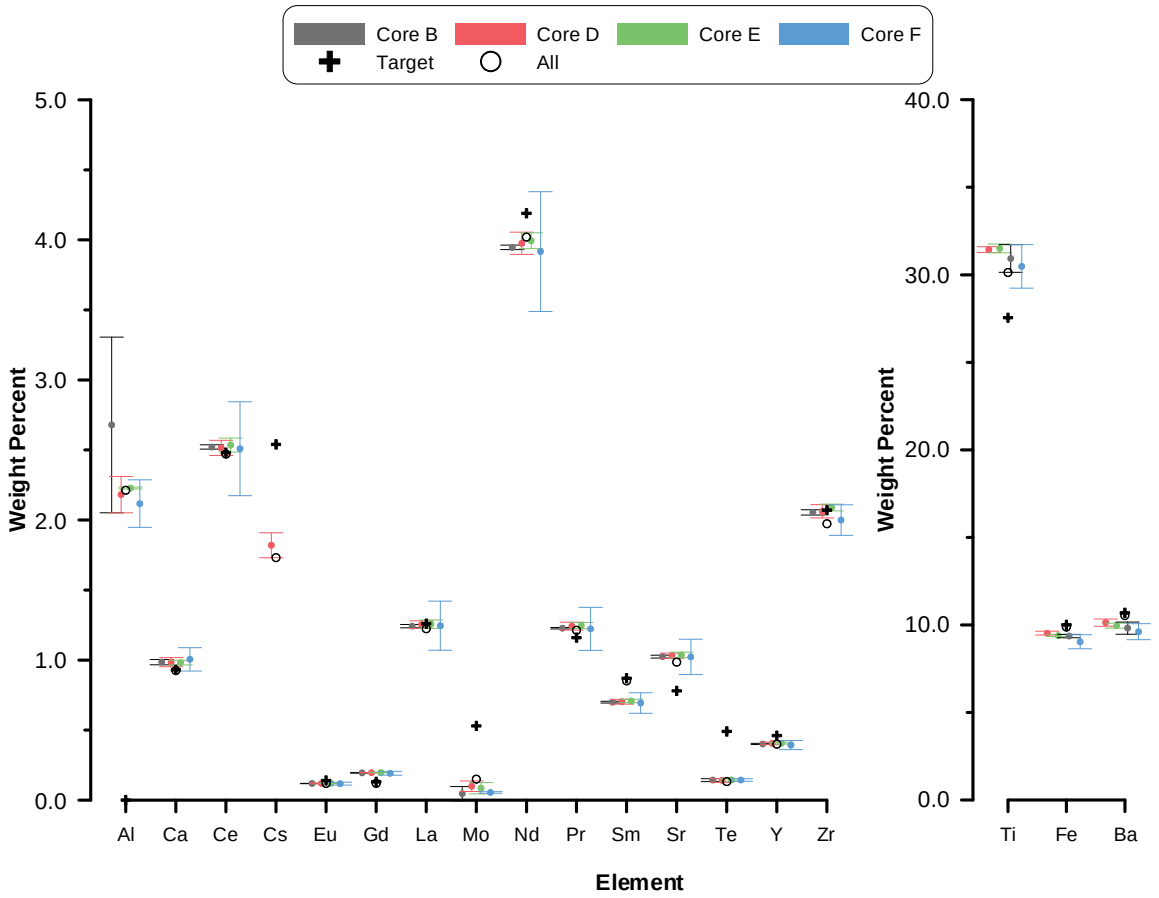

Figure 13. Plot of mean elemental concentrations and corresponding standard deviation from samples grouped according to radial distance. (D: center, E: ½ radius, F: edge, B: ½ radius)

[h] Additional statistical analysis was performed to determine the impact of Core F Zone 3 measurements on the ANOVA results of the Zone grouping. Core F Zone 3 was not found to bias the previous conclusions.

6.3.2 Fe RedOx

The redox state is of interest because reduced melts are known to have positive effects on the final properties of the ceramic.[14,16] Ti metal was added to the CCIM during initiation and it was expected that some amount of reduction was possible. Fe redox was measured on one sample, Core D, to determine the redox of the CCIM material. As with the other analyses, Fe redox was measured for different zones (morphology) within the core. The results, summarized in Table 10, indicated that the CCIM material was partially reduced (~20% Fe^{2+}).

Table 10. Measured Fe^{2+} Fraction in Core D

	Fe^{2+} / Fe Total
Zone 1	0.13
Zone 2	0.19
Zone 3	0.24
Zone 5	0.20

6.3.3 X-ray Diffraction

XRD confirmed three primary phases in the core samples as hollandite, pyrochlore, and zirconolite. Phase analysis conducted on the different morphologies observed in the individual cores indicated similar phase assemblage. In general, the XRD results indicate material in the CCIM was homogenous varying depths in the melt as well as radially from the center to the edge of the melt. XRD patterns for three cores positioned radially from the center of the melter are shown in Figure 14 and calculated phase abundances calculated from the XRD patterns are summarized in Figure 15. Included in Figure 15 is the estimated phase abundance based on the target composition and normalized for the three measured primary phases. In general, the estimated and measured phase information indicates the CCIM test was successful in producing a homogenous ceramic from a melt.

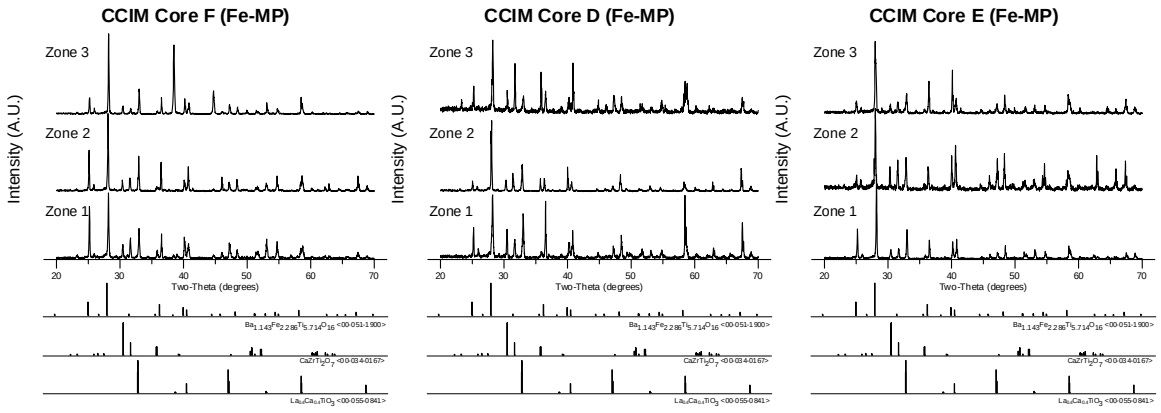

Figure 14. XRD patterns of Core E sample sections. Labeled patterns: Z1 = dense material, Z2 = columnar material, and Z3 = porous material.

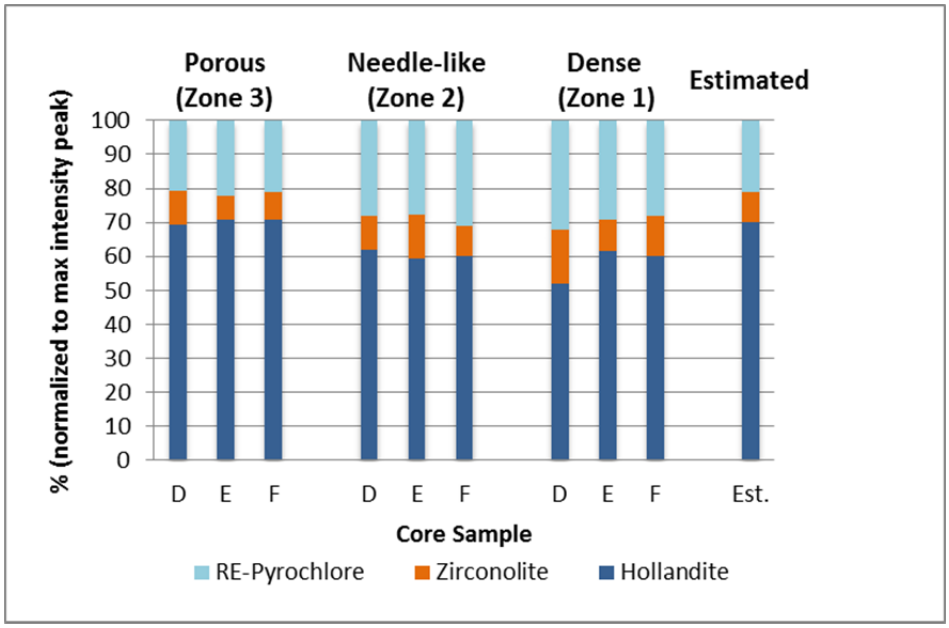

Figure 15. Summary of primary phase abundances in core samples compared to estimated abundances based on feed composition and target phase assemblage.

6.3.4 Chemical Durability

Chemical durability was performed to assess the relative durability of different areas from the CCIM material. Specifically, potential differences in durability throughout the bulk material were tested by sampling material from different Zones (similar to the chemical composition testing). The results of the aqueous durability testing are summarized in Figure 16. Element releases not shown in Figure 16 were below detection. Similar to composition data, the greatest standard error was observed in the Zone 3 and 5 samples suggesting that precise sampling in those areas is difficult or that those areas possess a greater degree of inhomogeneity. The durability results indicate Cs and Al elemental releases were practically equivalent across all zones. The Te elemental release exhibited comparatively more variation from each zone. Additionally, Zone 1 (dense) exhibited a higher Te release compared to the other zones. Mo exhibited the greatest variation from each zone than the other elements. Recalling the SEM/EDS results, Mo appears distributed throughout the ceramic, but it would appear not well chemically incorporated into primary phases. The distribution of Te was not determined because the characteristic x-ray energy of Te is similar to Ca making it difficult to identify using EDS. Nevertheless, Te also would appear not well incorporated into the matrix phases.

Given that the Fe-MP CCIM composition was not compositionally ideal, it follows that compositional adjustment could be used to better incorporate (increase durability) of various elements. Indeed, previous work has demonstrated that is the case. Together, this most recent CCIM test and the resulting characterization and demonstrated compositional improvements support the value in a CCIM test with an improved feed composition.

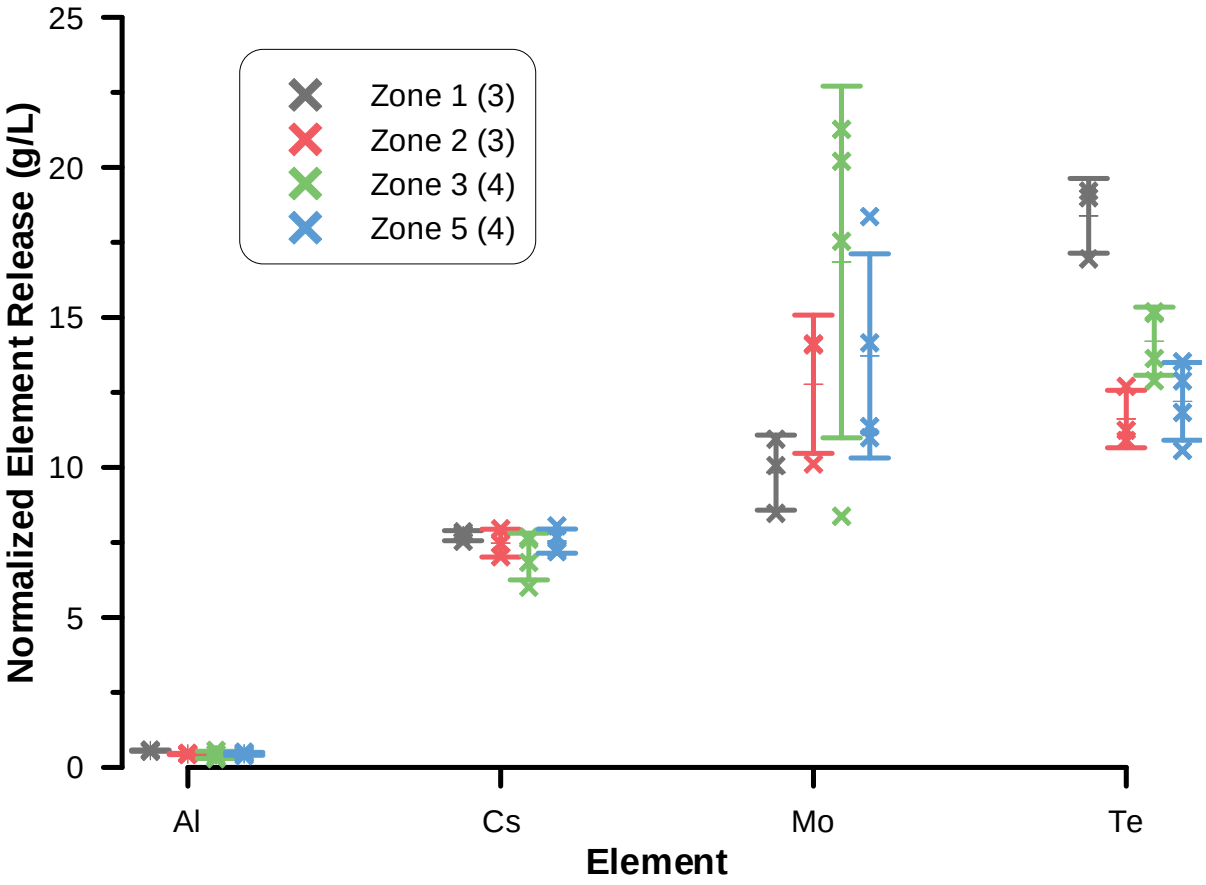

Figure 16. Normalized release for elements with measureable response after exposure to PCT. Individual samples are indicated with "x" and corresponding standard error bars are drawn.

7.0 Conclusions

Significant advances were made towards understanding melt processing ceramic waste forms for advanced nuclear fuel cycles. This work has demonstrated that future fuel cycle waste streams can be incorporated into crystalline ceramic waste forms by a melt and crystallization process. Ceramic waste forms based on Cr-containing hollandite were shown to promote hollandite formation which in turn promotes Cs incorporation. Cr preferentially enters the hollandite phase (even in the presence of competing phases) and, due to its refractory nature, is not easily reducible nor reactive with Cs, thereby serving to stabilize the hollandite phase. The targeted phases of hollandite, perovskite/pyrochlore, and zirconolite formed by a melt process are similar to those formed from solid state sintering alternatives such as Hot Pressing and Spark Plasma Sintering. The principal differences between the synthesis procedures are melt processing produced large-grain (order of magnitude larger for melt as compared to solid state processes) microstructures exhibiting greater compositional variety within individual phases and the bulk density (larger voids with melt process). The use of solid state buffer Ti/TiO_2 seems especially useful in promoting Cs incorporation into the hollandite phase and is recommended for use in subsequent melt processing trials. In fact, additives of Ti metal have been used to improve the electrical conductivity of powder batches in CCIM trials and therefore serve a dual use. Hollandite compositions with Cr additions are considered a promising phase for Cs-immobilization and are the basis for continued multiphase ceramic waste form development and testing.

The first scaled proof of principle test for processing multi-phase crystalline waste forms from a melt was completed using the CCIM at INL in October 2014. During this initial test, although the drain operation could not be completed, a ceramic was fabricated from a melt process for treating the HLW stream generated from an envisioned fuel cycle flow sheet. Characterization of material produced during the test indicated that the ceramic material exhibited a desirable phase assemblage consisting primarily of hollandite, zirconolite, and pyrochlore/perovskite phases. Characterization performed on the processed material confirmed that the ceramic was compositionally homogenous with similar phase abundances/assemblage. Similarly, durability testing indicated the material was homogeneous with no apparent correlation between Cs and Mo release, indicating that processing and compositional control effectively suppressed the formation of detrimental Cs-Mo containing compounds. This recent CCIM test and the resulting characterization in conjunction with demonstrated compositional improvements provide justification for future melt-processed ceramic waste form testing.

8.0 References

1. D. S. D. Gunn, N. L. Allan, H. Foxhall, J. H. Harding, J. A. Purton, W. Smith, M. J. Stein, I. T. Todorov and K. P. Travis, "Novel Potentials for Modelling Defect Formation and Oxygen Vacancy Migration in $Gd_2Ti_2O_7$ and $Gd_2Zr_2O_7$ Pyrochlores," *Journal of Materials Chemistry*, **22** [11] pp. 4675-4680, (2012).

2. R. Ubic, I. M. Reaney and W. E. Lee, "Perovskite $NdTiO_3$ in Sr- and Ca-doped BaO-Nd_2O_3-TiO_2 Microwave Dielectric Ceramics," *Journal of Materials Research*, **14** [04] pp. 1576-1580, (1999).

3. H. F. Xu and Y. F. Wang, "Crystallization Sequence and Microstructure Evolution of Synroc Samples Crystallized from $CaZrTi_2O_7$ Melts," *Journal of Nuclear Materials*, **279** [1] pp. 100-106, (2000).

4. V. Aubin-Chevaldonnet, D. Caurant, A. Dannoux, D. Gourier, T. Charpentier, L. Mazerolles and T. Advocat, "Preparation and Characterization of $(Ba,Cs)(M,Ti)_8O_{16}$ ($M = Al^{3+}$, Fe^{3+}, Ga^{3+}, Cr^{3+}, Sc^{3+}, Mg^{2+}) Hollandite Ceramics Developed for Radioactive Cesium Immmobilization," *Journal of Nuclear Materials*, **366** [1-2] pp. 137-160, (2007).

5. M. L. Carter, E. R. Vance and H. Li, "Hollandite-rich Ceramic Melts for Immobilization of Cs," *Mat. Res. Soc. Symp. Proc.*, **807** pp. 249-254, (2003).

6. M. L. Carter, E. R. Vance, D. R. G. Mitchell and Z. Zhang, "Mn Oxidation States in $Ba_xCs_yMn_zTi_{8-z}O_{16}$," *Mat. Res. Soc. Symp. Proc.*, **824** pp. CC4.6.1 - 6, (2004).

7. T. Advocat, G. Leturcq, J. Lacombe, G. Berger, R. A. Day, K. Hart, E. Vernaz and A. Bonnetier, "Alteration of Cold Crucible Melter Titanate-based Ceramics: Comparison with Hot-Pressed Titanate-based Ceramic," *Mater. Res. Soc. Symp. Proc*, **465** pp. 355-362, (1997).

8. I. A. Sobolev, S. V. Stefanovskii, B. I. Omelianenko, S. V. Ioudintsev, E. R. Vance and A. Jostons, "Comparative Study of Synroc-C Ceramics Produced by Hot-Pressing and Inductive Melting," *Mater. Res. Soc. Symp. Proc*, **465** pp. 371-378, (1997).

9. J. W. Amoroso and J. C. Marra, "Ceramic Waste Form Data Package: Fuel Cycle Research and Development," *US Department of Energy Report Office of Nuclear Energy Separations and Waste Forms Campaign SRNL-STI-2014-00247 (FCRD-SWF-2014-000581),* Savannah River National Laboratory, Aiken SC (2014).

10. S. E. Kesson, "The Immobilization of Cesium in SYNROC Hollandite," *Radioactive Waste Management and Environmental Restoration*, **4** [1] pp. 53-72, (1983).

11. C. Biagioni, P. Orlandi and M. Pasero, "Ankangite from the Monte Arsiccio mine (Apuan Alps, Tuscany, Italy): occurrence, crystal structure, and classification problems in cryptomelane group minerals," *Periodico Di Mineralogia*, **78** [2] pp. 3-11, (2009).

12. R. W. Cheary and J. Kwiatkowska, "AN X-RAY STRUCTURAL-ANALYSIS OF CESIUM SUBSTITUTION IN THE BARIUM HOLLANDITE PHASE OF SYNROC," *Journal of Nuclear Materials*, **125** [2] pp. 236-243, (1984).

13. M. L. Carter, E. R. Vance, D. R. G. Mitchell, J. V. Hanna, Z. Zhang and E. Loi, "Fabrication, characterization, and leach testing of hollandite, (Ba,Cs)(Al,Ti)(2)Ti6O16," *Journal of Materials Research*, **17** [10] pp. 2578-2589, (2002).

14. J. Amoroso, J. Marra, S. D. Conradson, M. Tang and K. Brinkman, "Melt Processed Single Phase Hollandite Waste Forms for Nuclear Waste Immobilization: Ba1.0Cs0.3A2.3Ti5.7O16; A = Cr, Fe, Al," *J. Alloys Compd.*, **584** pp. 590-99, (2014).

15. S. Wang, M. Tang, L. Zhang, G. Xiao, K. Brinkman and F. Chen, "Irradiation effect on the structure change for $Sr_2Fe_{1.5}Mo_{0.5}O_{6-\delta}$ perovskite ceramic " *J. Alloys Compd.*, **578** [25] pp. 170-75, (2013).

16. K. Brinkman, J. Amoroso, J. Marra and M. Tang, "Crystalline Ceramic Waste Forms: Comparison of Reference Process for Ceramic Waste Form Fabrication," *US Department of Energy Report SRNL-STI-2013-00442 (FCRD-SWF-2013-000229)*, Savannah River National Laboratory, Aiken SC (2013).